

dislocation pinning by a nanovoid in copper

Takahiro Hatano

Institute for Materials Research, Tohoku University, Sendai, 980-8577 Japan

(Dated: May 23, 2019)

Interaction between an edge dislocation and a void in copper is investigated by means of molecular dynamics simulation. It is found that the critical resolved shear stress (CRSS) at which depinning occurs logarithmically increases with void radius. The pinning angle, which characterizes the obstacle strength, approaches zero when the void radius exceeds 3 nm. Also, the distance between the void center and the glide plane is found to affect the pinning strength asymmetrically. Especially, dislocation is pinned even when it is not in contact with a void because of the strain field around the dislocation. Temperature and the shear deformation of void caused by the plastic flow are also found to be irrelevant to the pinning strength and CRSS.

PACS numbers: 61.80.Az, 62.20.Fe, 61.72.Qq

I. INTRODUCTION

Voids are usually generated in irradiated metals and act as obstacles to dislocation motion as well as other radiation-induced defects: e.g. stacking fault tetrahedra or Helium bubbles. The existence of those obstacles results in the rise of yield strength and plays an important role in hardening. To investigate the extent of hardening by those obstacles including voids, there have been a model in which dislocation is regarded as a continuous string of the uniform line tension. This is referred to as the string model. In the presence of obstacles, dislocation is fixed to form a cusp at an obstacle. The pinning angle ϕ is defined as the angle between two tangent vectors at a cusp. (See FIG. 1). Then the restoring force at the cusp to make the dislocation straight is written as $2\gamma \cos(\phi/2)$, where γ denotes the line tension. We assume that the dislocation can penetrate the obstacle when the restoring force exceeds the critical value. Since γ is a constant, this condition is equivalent to $\phi \leq \phi_c$, which we call the critical angle. Note that stronger obstacles have smaller critical angle. A dislocation bows out to form an arc between two obstacles until the pinning angle reaches the critical angle.

For a periodic array of the obstacles whose distance is L , the critical resolved shear stress τ_c above which the dislocation can penetrate the array of obstacles is represented by

$$\tau_c = \frac{2\gamma}{bL} \cos \frac{\phi_c}{2}, \quad (1)$$

where b and γ denote the burgers vector length and the

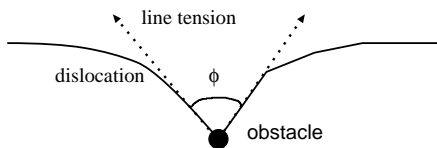


FIG. 1: A cusp formed at an obstacle. The angle ϕ between two tangential vectors is called the pinning angle.

line tension of the dislocation, respectively. (The line tension γ is given by the elastic theory and is often estimated to be $Gb^2/2$, where G represents the shear modulus.)

In more realistic situations, obstacles are distributed randomly on the glide plane and their randomness may play a crucial role in the dislocation motion. In order to incorporate this effect, Foreman and Makin performed computer simulation of dislocation motion in randomly distributed obstacles which have the same critical angle [1]. They found that the dislocation propagation has two qualitatively different modes depending on the critical angle [15]. For obstacles of small critical angle (i.e. strong obstacles), dislocations propagation resembles dendritic growth, while for large critical angle (i.e. weak obstacles) the global form of the dislocation does not significantly change from the straight line. Also τ_c are well described by

$$\tau_c = \begin{cases} \frac{2\gamma}{bL} \left(\cos \frac{\phi_c}{2} \right)^{\frac{3}{2}}, & \text{(for large } \phi_c \text{)} \\ \frac{1.6\gamma}{bL} \cos \frac{\phi_c}{2}, & \text{(for small } \phi_c \text{)} \end{cases} \quad (2)$$

where L denotes square root of the area density of obstacles on the glide plane [2]. This relation interconnects the microscopic quantity (ϕ_c) with macroscopic yield strength (τ_c), and has been used to evaluate the hardening [16].

In this context, the critical angle ϕ_c , which determines the obstacle strength, is an important parameter to discuss the extent of hardening due to obstacles. However, the estimation of the critical angle is not an easy task. We are unaware of any successful attempts for the theoretical calculation of ϕ_c . The difficulty involves the consideration of core structure of dislocation, since continuum elastic theory no longer applies. Meanwhile, in experiments, estimation of the critical angle requires high resolution both in space and in time (typically subnanometer and nanosecond scales). Besides, since subnanometer obstacles cannot be seen by transmitted electron microscopy, one cannot determine what obstacle pins the dislocation. In this regard, extensive molecular dynamics (MD) simulations on the interactions between dislocation and radiation-induced obstacles have been performed: e.g.

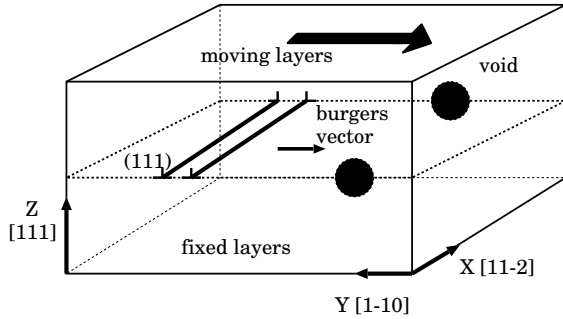


FIG. 2: Schematic of the system.

stacking fault tetrahedra [3], interstitial loops [4], copper precipitates in α -iron [5], etc. In this paper, along the line of the above simulation studies, we wish to estimate the critical angle for edge dislocation pinned by a void in copper. Note that we concentrate on the edge dislocation here. Simulations on the screw dislocation will be presented elsewhere.

This paper is organized as follows. In section II, we introduce the model: fcc copper including an edge dislocation and a void. In section III, void size dependence on the critical angle and the critical resolved shear stress is discussed. In section IV, effects of the distance between the void center and the glide plane where the dislocation moves are investigated. In section V, we discuss how the shear deformation of the void caused by the passage of dislocations affects α . Section VI is devoted to discussions and conclusions. In Appendix, we briefly summarize some peripheral results regarding the properties of α .

II. THE MODEL

A. the geometry

We treat fcc copper in this paper. As for the interatomic potential, the many-body potential of the Finnis-Sinclair type is used [6]. Parameters for copper are fitted by Ackland et al. [7] and have been widely used in many papers dealing with copper. The lattice constant $a = 3.615 \text{ \AA}$.

The schematic of our system is shown in FIG. 2. The x , y , and z axes are taken as the $[1\bar{1}\bar{2}]$, $[1\bar{1}0]$, and $[111]$ directions, respectively. The length in each dimension is 23 nm, 23 nm, and 15 nm. Periodic boundary conditions are employed in the x and the y directions. That is, we consider dislocations of infinite length in the x direction are periodically located in the y direction.

Note that we have the surface only in the z direction, both for $z > 0$ and for $z < 0$. Three atomic layers of $[111]$ next to the lowest surface ($z < 0$) are "the fixed layers" where velocities of the atoms always vanish. Similarly, three atomic layers of $[111]$ next to the upper surface ($z > 0$) are "the moving layers" where velocities of the

atoms are not given by the integration of force acting on them, but are given as a constant to cause the shear stress. Namely, the strain rate is the control parameter: not the shear stress. The moving surface moves to the $-y$ direction: i.e. $[1\bar{1}0]$.

In order to introduce a void, atoms whose barycentric positions are in the spherical region $(x \pm L/2)^2 + y^2 + z^2 < r^2$ are removed, where r denotes the radius of the void. To introduce edge dislocation, atoms belonging to one $(1\bar{1}0)$ plane and satisfies $z < 0$ are removed and the rest of the atoms are displaced by the strain field calculated from the elastic theory. This procedure produces a perfect edge dislocation whose burgers vector is $a/2[1\bar{1}0]$. However, a perfect dislocation in fcc crystals are energetically unstable to split into two partial dislocations whose burgers vector length b is $a/\sqrt{6} = 1.476 \text{ \AA}$.

$$\frac{a}{2}[1\bar{1}0] \rightarrow \frac{a}{6}[2\bar{1}\bar{1}] + \frac{a}{6}[1\bar{2}1]. \quad (3)$$

Since we wish to prepare two partial dislocations and a void in an initial system, atoms are suitably shifted from the original position by the steepest descent method in order to realize the dissociation. In addition, since our system consists of the periodic array of dislocations due to the periodic boundary conditions in the x direction, this procedure also incorporates the excess strain field caused by the next dislocations. After a certain time step, the perfect dislocation dissociates to yield two partial dislocations separated by approximately 2 nm.

Then, velocities are introduced by random numbers which obey the Maxwell-Boltzmann distribution. Temperature is fixed to be 300 K in this study. After a relatively short time required for phonon relaxation, "the moving layer", which is explained above, begins to displace to cause strain.

One should pay due attention to the instruction of Ostrowsky and Bacon [8] in preparing the dislocation system in atomistic scale simulations.

B. the strain rate

The strain rate $\dot{\epsilon}$ is an important parameter in MD simulations dealing with dislocations. In this paper, we set $\dot{\epsilon} = 8 \times 10^6 \text{ [sec}^{-1}\text{]}$. Although it seems still unrealistically fast deformation, the strain rate in MD simulation should not be directly compared with the macroscopic (or experimental) strain rate because the macroscopic strain rate involves only the average dislocation velocity. Namely, both spatial and temporal fluctuations in dislocation velocity are neglected. The complete correspondence of microscopic dislocation velocity to the macroscopic strain rate is not clear at all unless we know the statistical property of space-time fluctuation in dislocation motion [17].

Calculation of the shear stress is noteworthy. We define the shear stress as the forces in the y direction acting on the unit area of the moving layers and the fixed layers. In order to reduce dynamical effect due to the high

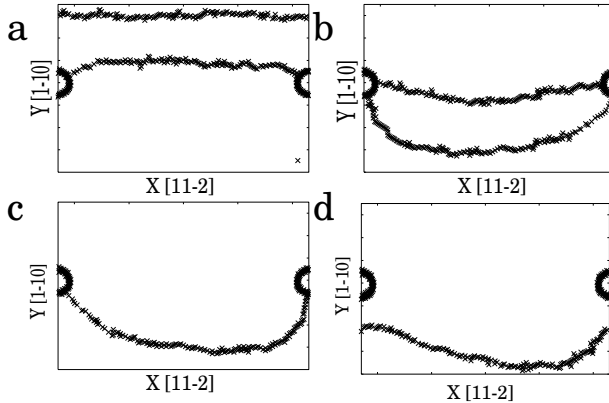


FIG. 3: Successive snapshots of the depinning process (a: 11 ps, b: 54 ps, c: 73 ps, d: 186 ps). Void radius is 1 nm. To visualize the void and the dislocations, only the atoms which constitute defects are presented by omitting atoms that have 12 nearest neighbors. (Atoms which form dislocations have 11 or 13 nearest neighbors, and the number of nearest neighbors of void surface atoms is less than 12.)

strain rate, simulation is performed twofold. Namely, the representative point in the phase space (spanned by the positions and the momenta of all atoms) are recorded every 4.6 ps. We then take the point where depinning just begins and restart the simulation but $\dot{\epsilon} = 0$. In this relaxation process, the shear stress relaxes to equilibrium value which we adopt as the critical shear stress. Without this relaxation process, the shear stress is too noisy for the discussion of quantitative behaviors.

III. VOID SIZE DEPENDENCE OF THE CRITICAL ANGLE AND THE CRITICAL RESOLVED SHEAR STRESS

First, we track the time evolution of the dislocation motion. By shearing the system, two partial dislocations move towards the $[1\bar{1}0]$ direction: the $-y$ direction. The burgers vectors of the leading and the trailing partials are $[\bar{2}1\bar{1}]$ and $[\bar{1}2\bar{1}]$, respectively. Pinning-depinning process is shown in FIG. 3. Note that there are two depinning processes corresponding to the leading and the trailing partials. The critical resolved shear stress and the pinning strength α is almost the same for the both partials, although the ones for the leading are slightly larger. We adopt the values for the trailing partial in the subsequent tables and graphs.

Then we calculate the critical angle and the critical resolved shear stress for various voids of four different radii: 0.3, 0.5, 1.0, and 1.5 nm. The critical angle is determined as follows. In correspondence with the string model where the uniform line tension is assumed, the dislocation is supposed to bow out as an arc. Then the

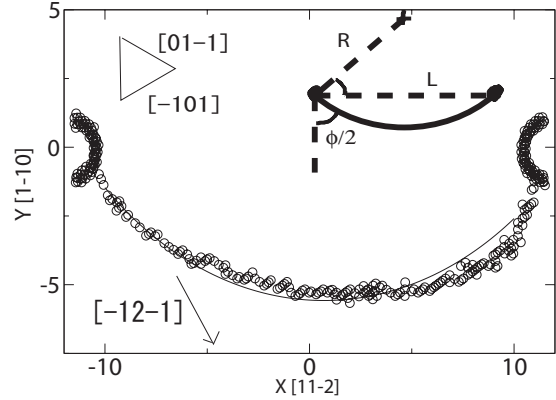


FIG. 4: Relation between ϕ_c and the curvature radius R .

TABLE I: void radius dependences of $\alpha = \cos(\phi_c/2)$ and the critical resolved shear stress (CRSS)

Void radius nm	α (nondimension)	CRSS MPa
0.3	0.38	47
0.5	0.50	63
1.0	0.72	83
1.5	0.80	95
2.5	0.91	106

shape of the dislocation is described as

$$y = \sqrt{R^2 - \frac{L^2}{4}} - \sqrt{R^2 - x^2} + r, \quad (4)$$

where R and r denote the curvature radius of the dislocation and the void radius, respectively. The curvature radius just before the depinning which is denoted by R_c is determined by fitting of the dislocation curve to Eq. (4) as shown in FIG. 4. Note that the bowing dislocation is well described by an arc, which means that the uniform line tension model is a good approximation. The pinning angle is then interrelated to the curvature radius by (see FIG. 4)

$$\cos \frac{\phi_c}{2} = \frac{L}{2R_c} \equiv \alpha, \quad (5)$$

where $\alpha = \cos \phi_c/2$ has the value in $[0, 1]$. In the strong pinning limit, $\alpha = 1$. If there is no pinning, $\alpha = 0$.

The values of α for different void radii are shown in TABLE. I together with the critical resolved shear stress τ_c . Surprisingly, the critical resolved shear stress obeys the empirical relation proposed by Bacon et al. [9];

$$\tau_c = A \log \frac{2r}{r_0(1 + \frac{2r}{L})}, \quad (6)$$

where A and r_0 denote the constant and the core cutoff of the elastic strain caused by the dislocation. The best fit is realized by letting $A = 33$ MPa and $r_0 = b$. In addition, we found that the relation of the same type holds for α :

$$\alpha = B \log \frac{2r}{r_0(1 + \frac{2r}{L})}, \quad (7)$$

where the proportional constant $B = 0.28$ fits the simulation result as shown in FIG. 5. We assume that B is independent of L and r . This assumption becomes important when we apply Eq. (7) to practical situations. By extrapolation, α reaches 1 when the void radius exceeds 3 nm, as shown in FIG. 5.

Combining Eq. (1), (6), and (7), we can estimate the line tension as

$$\gamma = \frac{bL}{2} \frac{A}{B} \simeq 0.21, \quad (8)$$

where the unit is nanoNewton [nN]. On the other hand, theory of dislocation based on the elastic mechanics estimates the line tension of the partial dislocation by decomposing its burgers vector into the edge component and the screw component:

$$\frac{a}{6}[\bar{1}2\bar{1}] = \frac{a}{4}[\bar{1}10] + \frac{a}{12}[11\bar{2}], \quad (9)$$

$$\equiv b_{\text{edge}} + b_{\text{screw}}. \quad (10)$$

Then the line tension reads

$$\gamma = \frac{G}{4\pi} \left(\frac{1}{1-\nu} b_{\text{edge}}^2 + b_{\text{screw}}^2 \right) \log \frac{R}{r_0}, \quad (11)$$

where ν , and R are the Poisson ratio and the outer cutoff of the elastic strain of the dislocation. The core cutoff r_0 near the dislocation is assumed to be 1 nm here. The outer cutoff R is set to be the distance to the next dislocation or to the surface, which is 10 nm in this simulation. Then the line tension is calculated as 0.26 nN, which approximately agrees with the above value Eq. (8). The slight discrepancy is not unreasonable because Eq. (11) is for the straight dislocation, while a curved dislocation involves in the present simulation.

However, they are much smaller than $\gamma = 0.54$ nN which corresponds to typical dislocation density, 10^{12} m⁻². Since the value of the line tension affects α , we have to consider the relation between the present simulation and experiments of much lower dislocation density. For that purpose, we recall the fact that depinning occurs when

$$2\gamma \cos(\frac{\phi}{2}) \geq 2\gamma\alpha. \quad (12)$$

Namely, $\gamma\alpha$ represents the intrinsic obstacle strength: not α alone. Then the relation between α 's which correspond to different line tensions (say γ_1 and γ_2) is given as $\gamma_1\alpha_1 = \gamma_2\alpha_2$. Then Eq. (7) is generalized as follows;

$$\alpha = \frac{0.059}{\gamma} \log \frac{2r}{b(1 + \frac{2r}{L})}. \quad (13)$$

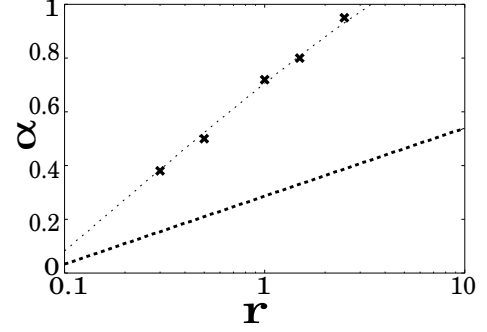


FIG. 5: Void radius dependences of α for the different line tensions. The simulation values which are shown in TABLE I are represented by \times . Thin dashed line represents Eq. (13) with $\gamma = 0.21$ and $L = 23$. Bold dashed line also represents Eq. (13) but with $\gamma = 0.54$ and $\frac{r}{L} \rightarrow 0$.

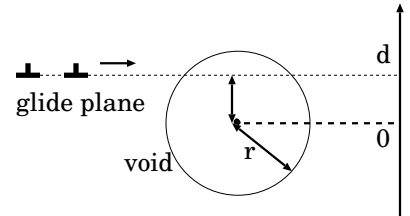


FIG. 6: The impact parameter d is defined by the distance from the void center to the glide plane. Note that the lower part of the void corresponds to the negative values of d .

If the line tension is larger, then α becomes smaller for the same void. For example, α for $\gamma = 0.54$ nN are shown in FIG. 5 using Eq. (13) with the assumption of $2r \ll L$. Although we have investigated only voids of $r \leq 2.5$ nm, by extrapolation, we can see that the value of α ranges from 0.3 to 0.5 for voids whose radii are few nanometers.

On the other hand, it should be stressed that the critical resolved shear stress is independent of the line tension, since τ_c is proportional to $\gamma\alpha$ (Eq. (1)), which is regarded as the intrinsic pinning strength.

IV. EFFECTS OF THE IMPACT PARAMETER

So far, we have limited ourselves to the situation where the dislocation penetrates the void center. This is rather a special case, for the relative position of a void to the glide plane on which the dislocation moves may be arbitrary. In this section, we change the distance between the void center and the glide plane. We call the distance "the impact parameter", which is denoted by d . (See FIG. 6.) The pinning strength α is determined for the various impact parameters by the same procedure with the last section.

The result is shown in FIG. 7, which shows asymmetric dependence of α on d . Note that the dislocation is pinned even when it is not in contact with the void. It

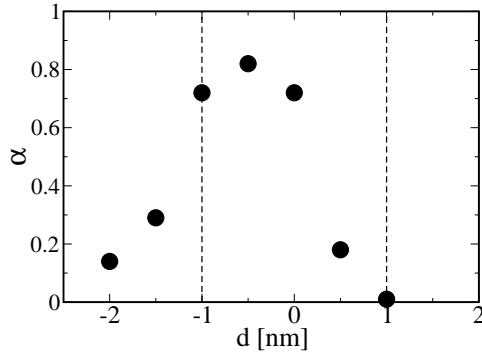


FIG. 7: Impact parameter dependence of the pinning strength α . Void radius is 1.0 nm (indicated by the dashed lines).

implies that, as well as the core energy, the elastic energy around the dislocation plays an important role in the pinning process. In addition, the asymmetry regarding $d = 0$ comes from the nature of strain field around the edge dislocation: i.e. the existence of hydrostatic pressure caused by the extra atomic plane. Especially, the fact that pinning strength for $d > 0$ becomes considerably weak suggests that the hydrostatic pressure is dominant over the shear stress. Therefore, the pinning of screw dislocations is expected to be much weaker due to the absence of hydrostatic pressure.

Also, we remark that strong pinning ($\alpha \geq 0.5$) occurs only where $-1.0r \leq d \leq 0$: i.e. the lower half of the void. This area accounts for approximately 30 or 40 percent of the whole pinning region, while the rest involves relatively weak pinning ($\alpha \leq 0.4$). The large variance of the pinning strength distribution for a single void suggests the reconsideration of the same pinning strength assumption in dislocation dynamics simulations.

V. EFFECTS OF VOID DEFORMATION AFTER THE PASSAGE OF SEVERAL DISLOCATIONS

When a void is passed by a dislocation, two parts which are divided by the glide plane are relatively displaced by its burgers vector. After the passages of several dislocations, it may collapse and lose the pinning ability. For example, the collapse of stacking fault tetrahedron by the passage of dislocations is both experimentally [11] and computationally [3] observed. This phenomenon is believed to be responsible for the formation of dislocation channel and the localization of the plastic flow, which recently invokes much attention including some computational study [10]. In this section, effects of the void deformation on dislocation pinning is discussed based on the motivation described above.

We remark that another possible mechanism for the void deformation is vacancy absorption by edge dislocations, which resulted in their climb motion. For example, Osetsky and Bacon [5] have found that the edge dislocation absorbs vacancies from the void in the MD simula-

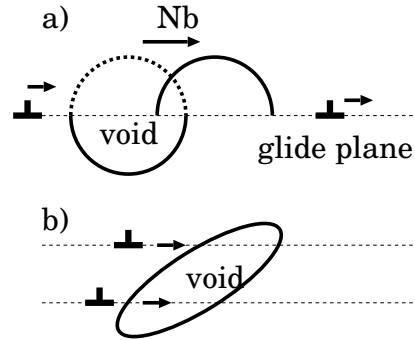


FIG. 8: Schematic of the void deformation by the passages of N edge dislocations: a) There is a single glide plane which cuts the void center. b) Glide planes are uniformly distributed. Each plane has N dislocations which are to penetrate the void.

tion of α -iron. However, no climb motion was seen in our simulations, because the climb of dislocation is difficult in fcc metals due to its dissociation. Hence, we do not consider the void contraction by the vacancy emission to dislocations. We concentrate on the effect of the relative deformation with respect to the glide plane.

We prepare the deformed void as shown in FIG. 8. First we prepare a spherical void. Then, instead of iterating the pinning simulations, atoms located above the glide plane are displaced by the burgers vector $a/2[\bar{1}10]$. Iterating this procedure for N times is equivalent to the passage of N edge dislocations. We set two configurations. In case (a), the glide plane on which the dislocations move is assumed to be at the void center, whereas the glide planes are uniformly distributed in case (b).

In case (a), we set $N = 5$ and $N = 10$. Namely, the void is assumed to be penetrated by dislocations on the same glide plane 5 times or 10 times. The pinning strength α is found to be 0.7 for the both cases, which is the same value with the one for the spherical void. This is consistent with the result obtained in the last section that the upper part of the void is dominant in pinning of edge dislocations because of the hydrostatic pressure.

In case (b), we test $N = 2$ and cannot find any difference from the undeformed case. Thus, as far as the vacancy absorption mechanism (i.e. dislocation climb) is absent, the pinning strength is not altered by the passage of dislocations.

VI. DISCUSSIONS AND CONCLUDING REMARKS

A. practical applications

Let us estimate the critical resolved shear stress for copper in which voids are randomly distributed. First, we determine the average spacing between obstacles on the glide plane, L . When the number density of voids

per unit volume is written as ρ , it is usually estimated that $L = 1/\sqrt{2r\rho}$. However, this expression includes all of the voids which intersects the glide plane and hence their impact parameters are randomly distributed from $-r$ to r . On the other hand, in the section IV we have seen that the pinning strength α considerably changes with the impact parameter. In order to incorporate this result, we will neglect the weak pinning although it may be a rough approximation. From FIG. 7, strong pinning ($\alpha \geq 0.4$) occurs only where $-1.2r \leq d \leq 0.2r$. Neglecting the rest, it is assumed that only the above region is responsible for pinning. That is, we use $1.4r$ instead of the diameter $2r$, which results in $L \simeq 1/\sqrt{1.4r\rho}$. Then Eq. (2) is rewritten as

$$\tau_c = \frac{2\gamma\alpha^{\frac{3}{2}}}{b} \sqrt{1.4r\rho}, \quad (14)$$

where the line tension γ should be suitably determined according to the dislocation density of the specimen. Once γ is determined, we can evaluate the corresponding α by using Eq. (13).

Now we are ready to estimate the extent of hardening from γ , ρ , and r . For example, dislocation density is assumed to be 10^{12} m^{-2} , which yields $\gamma = 0.54 \text{ nN}$. When the voids where $2r = 4.1 \text{ nm}$ are scattered in bulk copper with the number density $\rho = 2.9 \times 10^{22} \text{ m}^{-3}$, we get $\alpha = 0.29$ and $\tau_c = 14 \text{ MPa}$. (The average spacing of obstacles $L \simeq 110 \text{ nm}$.)

B. comparison with the continuous model with self-interaction

Bacon et al. [9] have represented the interesting theory of Orowan process based on the continuous model incorporating the self-interaction of dislocation. Their system consists of the periodic array of impenetrable obstacles. It is rather striking that the Orowan stress obtained there shows the same tendency with ours, Eq. (6), despite of the different nature of the obstacles and the calculation methods.

Let us briefly review their discussion. They have speculated that, at the Orowan stress, the effective line tension γ_{eff} of largely bowing edge (screw) dislocation is equal to that of the straight screw (edge) dislocation. Then the Orowan stress τ_{Orowan} is represented using the effective line tension.

$$\tau_{\text{Orowan}} = \frac{2\gamma_{\text{eff}}}{Lb} \quad (15)$$

$$\gamma_{\text{eff}} = \frac{Gb^2}{4\pi} \log \frac{\bar{R}}{\bar{r}_0}, \quad (16)$$

where \bar{R} and \bar{r}_0 denote the effective cutoffs for bowing dislocation. The outer cutoff \bar{R} is estimated as

$$\frac{1}{\bar{R}} = \frac{1}{L-2r} + \frac{1}{2r}, \quad (17)$$

while the core cutoff \bar{r}_0 is suitably fitted (approximately $2b$). Although the above discussion was quite rough and heuristic, Eq. (17) applies to the result obtained in this paper.

However, in our simulation, γ_{eff} is estimated to be a constant independent of r . Instead, α shows the logarithmic dependence: Eq. (7) and FIG. 5. In Bacon, $\alpha \simeq 1$ regardless of r and L , since impenetrable obstacles are treated. The difference comes from the extent of bow-outs. In our simulation, the maximum displacement of dislocation in the y direction is approximately $0.25L$, whereas $0.59L$ in Bacon. (The ratio r/L is almost 0.05 in the both cases.) Thus, the line tension changes by the dislocation self-interaction for impenetrable obstacles, while α changes for penetrable obstacles.

C. conclusion

We calculated the critical pinning angle ϕ_c for the interaction between voids and the edge dislocation in fcc copper. The pinning strength $\cos(\phi_c/2)$ and the critical resolved shear stress obey the empirical relations similar to the one which Bacon et al have found. Also we found that the pinning angle strongly depends on the line tension which is a function of the dislocation density, and proposed the correction to this effect. The distance between the void center and the glide plane is found to affect the pinning strength. Combining those results, the estimation of the critical resolved shear stress becomes possible from the values of the line tension of dislocation and the number density and the radius of voids.

Of course, these results are confined to edge dislocations. The pinning strength α for screw dislocation is naively expected to be larger than that for edge dislocation, since the line tension of screw dislocation is smaller. However, for their strain field is different from each other, the nature of pinning might be different. For example, the asymmetry with respect to the impact parameter which is investigated in section IV is not expected for the screw dislocation case. Another simulation on screw dislocation is in progress to investigate its pinning properties, which will be presented elsewhere.

The impact parameter dependence of the critical angle also suggests the importance of randomness in continuous models. Even if the system contains voids of almost the same radius, its cross section to the glide plane is randomly distributed. Hence we have to incorporate the randomness in the pinning strength. It is not straightforward to deduce this effect from the existing simulations which treats only two kinds of obstacles [12]. Investigation of a continuous model with random pinning angles would be interesting to see how the impact parameter dependence affects the macroscopic dislocation motion.

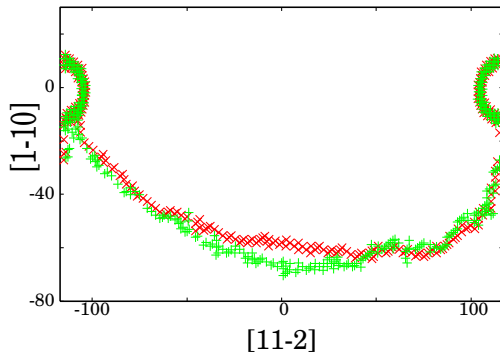


FIG. 9: Snapshots of dislocations just before depinning. \times denotes the simulation of 100 K, and $+$ denotes the one of 500 K. The subtle difference in the middle lies in the range of thermal fluctuation of dislocations.

Acknowledgments

The author gratefully acknowledges N. Nita for useful discussions regarding experimental situations. He also thanks Y. Sato and H. Matsui for discussions and valuable comments.

APPENDIX A: TEMPERATURE DEPENDENCE

As one of the peripheral results, we introduce the temperature dependence of the pinning strength α and CRSS. We have recalculated α and CRSS following the same procedure described in the sections II and III but with different temperatures: 100 K, 200 K, 400 K, and 500 K. We cannot find any differences between these calculations and the one for 300 K. In FIG. 9 we show the snapshots of the dislocations just before depinning where the temperature is 100 K and 500 K, respectively. We can see no difference in the pinning strength, and the CRSS is almost the same. Namely, temperature plays no role in depinning processes.

The reason is that the activation energy is too large compared with the thermal energy of the involved atoms around the void. Although a precise estimation for the activation energy is difficult, it is at least larger than the energy of the dislocation whose length is equivalent to the void diameter. (We neglect the step formation energy on the void surface). Dislocation energy is calculated by the line tension multiplied by the length. Note that the line tension is estimated to be 0.21 nN in Eq. (8). Therefore,

for the void of 2.0 nm radius, the activation energy is estimated as 4.2×10^{-19} J. It is equivalent to $10^4 k_B T$, where k_B denotes the Boltzmann constant and $T = 300$ K. Since this is much larger than the thermal energy of involved atoms (less than a hundred), it is plausible that thermal fluctuations cannot assist dislocation depinning. (Please recall that the step formation energy is neglected and the actual value may be larger than that.)

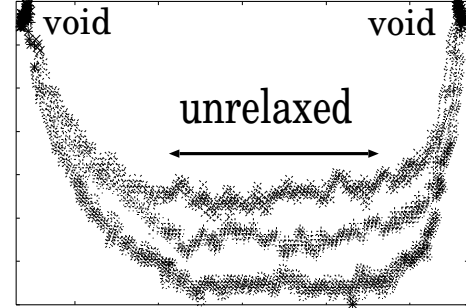


FIG. 10: Three snapshots showing the relaxation of dislocation line. The distance between voids is 53 nm. The strain rate is 8×10^6 s $^{-1}$. The duration between each snapshot is 900 ps. The area indicated as "unrelaxed" forms almost straight line which is to relax into arc very slowly. Just after the third snapshot, depinning occurs before the total relaxation. Namely, the middle area of the dislocation is still straight at depinning.

APPENDIX B: ON THE SLOW RELAXATION OF THE LINE TENSION

The uniform line tension approximation concludes that bowing dislocations form arc, which is approximately realized as shown in FIG. 4. However, this can hardly be realized in MD simulations when the spacing between voids becomes larger. Spatial relaxation of the line tension is limited by thermally activated jumps of dislocation segments over the Peierls potential. Henceforth, the curvature localizes near the void and depinning occurs before the dislocation relaxes into the arc. This leads to the overestimation of α .

In FIG. 10, we show the relaxation pattern for the case of $L = 53$ nm. Note that the relaxation becomes slower for lower temperatures. Therefore, it takes much smaller the strain rate for the estimation of α when we will treat larger systems. In this regard, the bowing dislocations calculated by Osetsky and Bacon [5] seem to be unrelaxed.

[1] A. J. E. Foreman and M. J. Makin, *Phil. Mag.* (1966).
[2] U. F. Kocks, *Can. J. Phys.* **45**, 737 (1967).
[3] B. D. Wirth, V. V. Bulatov, and T. Diaz de la Rubia, *J. Eng. Mater. Tech.* **124**, 329 (2002).
[4] D. Rodney and G. Martin, *Phys. Rev. Lett.* **82**, 3272 (1999).
[5] Yu. N. Osetsky and D. J. Bacon, *J. Nucl. Mater.* **323**, 268 (2003); *Phil. Mag.* **83**, 3623 (2003).
[6] M. W. Finnis and J. E. Sinclair, *Phil. Mag. A* **50**, 45 (1984).

- [7] G. J. Ackland, D. J. Bacon, A. F. Calder, and T. Harry, *Phil. Mag. A* **75**, 713 (1997).
- [8] Yu. N. Ossetsky and D. J. Bacon, *Modell. Simul. Mater. Sci. Eng.* **11** 427 (2003)
- [9] D. J. Bacon, U. F. Kocks, and R. O. Scattergood, *Phil. Mag.* **28**, 1241 (1973).
- [10] T. D. de la Rubia, H. M. Zbib, T. A. Khraishi, B. D. Wirth, M. Victoria, and M. J. Caturla, *Nature* **406**, 871 (2000).
- [11] Y. Matsukawa, Yu. N. Ossetsky, R. E. Stoller, and S. J. Zinkle, in *Fusion Materials Volume 36*, (Semiannual Progress Report for Period Ending June 30, 2004, Oak Ridge National Laboratory) pp. 98 (2004).
- [12] A. J. E. Foreman and M. J. Makin, *Can. J. Phys.* **45**, 511 (1967).
- [13] M. Cieplack and M. O. Robbins, *Phys. Rev. B* **41**, 11508 (1990); *Phys. Rev. Lett.* **60**, 2042 (1988).
- [14] J. Marian, W. Cai, and V. V. Bulatov, *Nature Mater.* **3**, 158 (2004)
- [15] The existence of the two modes in one-dimensional surface propagation was rediscovered by Cieplak and Robbins [13] in the context of fluid invasion in porous media.
- [16] The validity of the definition of critical resolved shear stress in the dendritic-growth mode is questionable.
- [17] At least in the strain rate discussed here, dislocation motion does not seem to be the iterations of kink pair formation and its propagation along the dislocation line. Actually it moves in the uniform manner by the strong shear stress where the Peierls potential becomes irrelevant. This thermal-athermal transition in dislocation motion due to the magnitude of applied shear stress was discussed by Marian et al. via MD simulation [14].